

The *Ulysses* Supplement to the BATSE 3B Catalog of Cosmic Gamma-Ray Bursts

K. Hurley

University of California, Berkeley, Space Sciences Laboratory, Berkeley, CA 94720-7450

M. S. Briggs, R. M. Kippen

University of Alabama in Huntsville, Huntsville AL 35899

C. Kouveliotou¹, C. Meegan, G. Fishman

NASA Marshall Space Flight Center, Huntsville AL 35812

T. Cline

NASA Goddard Space Flight Center, Code 661, Greenbelt, MD 20771

M. Boer

Centre d'Etude Spatiale des Rayonnements, B.P. 4346, 31029 Toulouse, France

ABSTRACT

We present Interplanetary Network localization information for 218 gamma-ray bursts in the 3rd BATSE catalog, obtained by analyzing the arrival times of these bursts at the *Ulysses* and *Compton Gamma-Ray Observatory* (CGRO) spacecraft. For any given burst observed by these two spacecraft, arrival time analysis (or “triangulation”) results in an annulus of possible arrival directions whose half-width varies between 7 arcseconds and 32 arcminutes, depending on the intensity and time history of the burst, and the distance of the *Ulysses* spacecraft from Earth. This annulus generally intersects the BATSE error circle, resulting in an average reduction of the error box area of a factor of 30.

Subject headings: gamma-rays: bursts; catalogs

1. Introduction

A knowledge of the precise positions of cosmic gamma-ray bursts (GRBs) is important for many studies. For example, recent observations of the optical counterparts to bursts have provided evidence that at least two of them are at cosmological distances (Metzger et al. 1997, Kulkarni et al. 1998) and that, by implication, most or all of them may also be. One optical counterpart has

¹Universities Space Research Association, Marshall Space Flight Center ES-84, Huntsville, AL 35812

been associated with a galaxy, and the majority of the models for the energy release in bursts have long invoked neutron star-neutron star or neutron star- black hole mergers (e.g. Paczynski 1991). If this is correct, GRBs should originate in or close to galaxies, and correlations between burst positions and the large scale structure of the universe might be expected. In this context, it has been debated whether the positions of bursts are correlated with those of Abell clusters (Kolatt & Piran 1996; Hurley et al. 1997a; Struble & Rood 1997) and radio-quiet quasars (Hurley et al. 1997b; Schartel, Andernach, and Greiner, 1997). In both cases, increased precision in the location accuracy leads to more stringent tests. Similarly, precise positions greatly improve searches for quiescent counterparts to GRBs in other wavelength ranges (e.g. Tokanai et al. 1997), and can help confirm proposed associations between GRBs and fading counterparts (Hurley et al. 1997c). Finally, burst recurrence from a single source is excluded in most cosmological models. Such recurrence would reveal itself through small-scale clustering in the angular distribution of burst locations, and the sensitivity of the distribution function to repeating sources is greater when the burst location accuracy is improved (Kippen, Hurley, & Pendleton 1998).

We present here a catalog of 218 gamma-ray bursts from the detector aboard the *Ulysses* spacecraft, which were also observed by the Burst and Transient Source Experiment (BATSE), and cataloged in the 3rd BATSE catalog (Meegan et al. 1996). In the present catalog, their positions have been improved in accuracy by arrival time analysis, or “triangulation”. Detection of an event by these two widely separated instruments leads to a narrow annulus which intersects the BATSE error circle and reduces its area by a factor of ≈ 30 . Such annulus/error circle intersections have played important roles in the examples cited above.

2. Instrumentation

The *Ulysses* GRB detector (Hurley et al. 1992) is one instrument in the 3rd Interplanetary Network of burst detectors. It consists of two 3 mm thick hemispherical CsI scintillators with a projected area of about 20 cm^2 in any direction. The detector is mounted on a magnetometer boom far from the body of the spacecraft, and therefore has a practically unobstructed view of the full sky. Because the *Ulysses* mission is in interplanetary space, the instrument also benefits from an exceptionally stable background. The GRB detector operates continuously, and over 97% of the data are recovered.

A unique feature of the mission is the fact that it is in heliocentric orbit with aphelion ≈ 5 AU. Thus it reaches an apogee of ≈ 6 AU or 3000 light-seconds, and during portions of the orbit, the GRB experiment is farther than any burst detector has ever been from Earth, resulting in greatly improved location accuracies for gamma-ray bursts.

The GRB instrument observes bursts in both a triggered and a real-time mode. The triggered mode is initiated when the number of counts in one of two possible time intervals exceeds a preset value. Because the background is stable, this number is defined in terms of an absolute number of

counts, rather than a number of standard deviations above the background. The two time intervals may be selected among values from 0.125 to 4 s. Each of the two time intervals is associated with an independently selectable energy window, whose lower and upper thresholds lie between ≈ 15 and 150 keV. The data collected in the triggered mode consist of energy spectra, and either 16 s of 8 ms count rates, or 64 s of 32 ms count rates, in the ≈ 25 to 150 keV energy range; ≈ 1.8 and 7.4 s of the data stream record the time histories prior to trigger, respectively. Following a trigger, data are read out for ≈ 40 m, during which time the experiment cannot re-trigger. An example is shown in Figure 1.

Independent of the trigger, a continuous stream of real time data is transmitted. This consists of count rates taken with 0.25, 0.5, 1, or 2 s time resolution. The resolution depends on the spacecraft telemetry rate, and the energy range is ≈ 25 to 150 keV, as for the trigger. Data are compressed in this mode. An example is shown in Figure 2. The real time data serve many purposes. For example, numerous gamma-ray bursts which are not intense enough to trigger the detector can be reliably identified in the real time data, as we demonstrate below. Bursts arriving during trigger readout may also be identified. Finally, bursts whose duration exceeds the duration of the triggered memory can be fully recorded in this mode.

BATSE consists of eight detector modules situated at the corners of the *Compton Gamma-Ray Observatory* spacecraft. Each contains a Large Area Detector (LAD), a 50.8 cm diameter by 1.27 cm thick NaI scintillator. The trigger algorithm examines the count rates of two or more detectors in the 50 - 300 keV energy range, over 64, 256, and 1024 ms intervals. The experiment is described in more detail in Meegan et al. (1996). For most of the events in this catalog, we have utilized the DISCSC and PREB data types summed over two, three, or four detectors. This gives a 0.064 s resolution time history from 2 seconds prior to the trigger to 240 s or more after the trigger. We select discriminator channels 1 and 2, corresponding to the energy range 25 - 100 keV, to match the *Ulysses* energy range as closely as possible. Rarely, this data type is not available; in that case we use MER, TTS, TTE, or 1 s resolution data. As BATSE is in low Earth orbit, the time history data are occasionally interrupted by data gaps and Earth occultation.

3. Search Procedure

Every cosmic burst detected by BATSE is systematically searched for in the *Ulysses* data as soon as the BATSE data are available for it. This is done by using the approximate arrival direction from BATSE and the position of the *Ulysses* spacecraft to calculate a range of possible arrival times at *Ulysses*. The calculation assumes generous uncertainties in the arrival direction to assure that the crossing window always includes the burst. Typical window lengths are 300 - 500 s (e.g., Figure 2). In cases where the BATSE positions undergo substantial revision, a revised search window is calculated and the search is redone.

To carry out the search, the *Ulysses* real time count rates are extracted for the crossing

window and plotted. The data are searched both automatically and by eye. In the automatic procedure, the background count rate is typically calculated over ten time intervals, and a $> 4\sigma$ increase is searched for over 2 or more consecutive time intervals. The search by eye confirms the presence of the increase, and in some cases, identifies increases that were not detected in the automatic procedure due, for example, to a long rise time. If the burst is intense enough to trigger the *Ulysses* GRB detector, burst detection is usually immediately apparent in both the real time and the triggered data streams, with one noteworthy exception. Very short bursts (durations < 0.25 s) can trigger, but remain difficult to identify in the lower time resolution real time data. Conversely, long bursts which do not reach large peak intensities can be identified in the real time data, but may not trigger regardless of their time-integrated fluxes.

4. Deriving Annuli by Comparing BATSE and *Ulysses* Time Histories

When a GRB arrives at two spacecraft with a delay δT , it may be localized to an annulus whose half-angle θ with respect to the vector joining the two spacecraft is given by $\cos\theta=c\delta T/D$, where c is the speed of light and D is the distance between the two spacecraft. (This assumes that the burst is a plane wave, i.e. that its distance is much greater than D .) The annulus width $d\theta$, and thus one dimension of the resulting error box, is $c\sigma(\delta T)/D\sin\theta$ where $\sigma(\delta T)$ is the uncertainty in the time delay. This term has two components, one statistical and one systematic. The first is associated with the uncertainty in comparing the time histories of a burst recorded by two different instruments; the second is due to the uncertainty in the clock calibrations of the two spacecraft. A third source of error is the uncertainty in the knowledge of the spacecraft positions. We discuss each in turn.

In the simple case of identical detectors with identical backgrounds, the most probable delay δT and its error $\sigma(\delta T)$ may be estimated as follows. Denote the two background-subtracted time histories by $X_i, Y_i, i=1,\dots,m$, that is, X_1 is the number of counts in the first time bin for detector X, and Y_1 the number of counts in the first time bin for detector Y, and so on. Assume that the background can be estimated with arbitrary accuracy, and further that each value of X_i and Y_i is an independent normal random variable with variance X_i and Y_i respectively. For simplicity of notation, assume that the two time histories recorded by detectors X and Y are perfectly aligned when time bin 1 of detector X corresponds to time bin 1 of detector Y. Then for this perfect alignment, corresponding to zero lag between the two time histories, the quantity $R_i = (X_i - Y_i)/\sqrt{X_i + Y_i}$ is a random variable with mean zero and variance unity for every i . Thus

$$\sum_{i=1}^n R_i^2 \tag{1}$$

is distributed as χ^2 with n degrees of freedom. Here the sum is performed over some number n of time bins, where $n \leq m$. Now allow the lag to vary slightly about zero, so that time bin i of detector X corresponds to time bin j of detector Y, and form the random variable

$R_{ij} = (X_i - Y_j)/\sqrt{X_i + Y_j}$ where the lag ij is now variable. The quantity

$$r_{ij}^2 = \sum R_{ij}^2 \quad (2)$$

where the summation is over the intervals which X and Y have in common, is similarly distributed as χ^2 . In practice we do not know *a priori* the lag at which the best correlation will occur, so we test various lags ij until r_{ij}^2 reaches a minimum, r_{min}^2 . Then the lag or time delay corresponding to a 3σ equivalent confidence level is $r_{ij}^2 = r_{min}^2 + 9$. (All annuli in this catalog have widths corresponding to 3σ equivalent confidence.)

Although this simple example describes the essential features of the method, there are numerous complicating factors in practice. For BATSE, the background varies over the orbit, and its value may not always be known accurately; the assumption of a normal distribution may also be violated when Cyg X-1 is in the field of view. The BATSE and *Ulysses* detectors have different areas, burst and background count rates, and time resolutions. We treat this by first, normalizing the BATSE background- subtracted time history to the *Ulysses* one so that two time histories have the same total number of counts. We also generate a BATSE time history with identical time resolution to the *Ulysses* one by scaling the counts in the original BATSE time bins. These adjustments complicate the above expressions considerably. However, through Monte-Carlo simulations, as well as time history comparisons using a completely different method (Laros et al. 1998), we have verified that the procedure gives correct results. In addition to calculating the r_{ij}^2 statistic, we also compute the correlation coefficient as a function of lag, namely

$$\rho_{ij} = \frac{\sum(X_i - \langle X \rangle)(Y_j - \langle Y \rangle)}{\{\sum(X_i - \langle X \rangle)^2 \sum(Y_j - \langle Y \rangle)^2\}^{0.5}}$$

where the summations are over the intervals that X and Y have in common, and find its maximum value. The purpose of this calculation is to assure that the r_{ij}^2 statistic has indeed identified the best lag; we require that the maximum ρ_{ij} and the minimum r_{ij}^2 correspond to identical lags, or at worst, that the difference between the lags be much less than the 3σ confidence interval. Finally, parabolic fits are done to both statistics to identify the best lag and the confidence intervals. An example is shown in Figures 3 and 4.

The second uncertainty, due to the clock calibrations, is in principle much smaller than the 3σ confidence interval. The clock on the *Compton Gamma-Ray Observatory* is accurate to 100 μ s, and this accuracy is verified through pulsar timing. Onboard software increases the uncertainty in the BATSE trigger times to ≈ 1 ms. The clock on the *Ulysses* spacecraft is calibrated during each daily tracking pass, and the clock drift is extrapolated until the next pass to obtain the correct time; the calibration is verified at six month intervals by sending commands to the GRB experiment at precisely known times. The exact procedure is described in Hurley (1994). Due to spacecraft buffering of the commands, the result is that *if* it can be assumed that no errors larger than 125 ms are present, *then* the clock can be shown to be accurate to several milliseconds. For the purposes of triangulation, however, we take the extremely conservative approach that no 3σ cross-correlation uncertainty is less than 125 ms. Larger timing errors have been identified in the

past for both missions. The *CGRO* clock was found to have a consistent 2 s offset in the early part of the mission, and random timing errors between 0.25 and several hundred seconds occurred in certain types of *Ulysses* data. In all cases the data were reprocessed to obtain the results in this paper.

Finally, the uncertainties in the spacecraft ephemerides are truly negligible. The *Ulysses* range is known to ≈ 10 km, and the right ascension and declination of the spacecraft are accurate to ≈ 0.00003 degrees. The GRO range is known to better than 50 km, and the right ascension and declination to better than 0.01 degrees. The error that these uncertainties produce in the knowledge of the interspacecraft vector (i.e., the center of the annulus) is of order 0.0005 degrees, and therefore usually two orders of magnitude smaller than the timing uncertainties. As a conservative measure, this uncertainty is added linearly to the uncertainties in the annulus parameters caused by the timing. It typically increases the annulus width by several tenths of an arcsecond.

The radius of each annulus and its right ascension and declination are transformed to a heliocentric frame. This is equivalent to an aberration correction (maximum value ≈ 20 arcseconds), and involves two adjustments. The first is to the spacecraft time. The signal from a distant spacecraft may travel several thousand seconds on its way to Earth. Depending on the Earth's velocity vector relative to the spacecraft, the relative motion of the Earth and the spacecraft may not be negligible during this period. "Geocentric" clock times are related to the position of the Earth when the signal is *received* from the spacecraft. "Heliocentric" clock times, i.e., times related to the position of the Earth when the signal was *transmitted*, must be used. The difference between the two may be as large as several hundred milliseconds, and is often comparable to or greater than the statistical uncertainty of the time history comparison. The second adjustment is to the inter-spacecraft vector. Two observers moving with the Earth and with the sun see different vectors (i.e., annulus centers) as a result of their motions during the burst's transit time between the two spacecraft. This correction, too, may not be negligible. The result of triangulating the 1993 January 31 burst is shown in Figure 5.

Although there have never been more than three widely separated spacecraft in the 3rd IPN, which would have provided redundant determinations and therefore a verification of burst positions, there have been numerous instances where a burst source with a known position was triangulated with *Ulysses*, BATSE, and other spacecraft. These include the soft gamma repeater SGR1806-20 and the bursting pulsar GRO J1744-28 (Hurley et al. 1996, 1998a), the 1997 January 11 burst localized by BeppoSAX (Galama et al. 1997), the 1997 February 28 burst, with both a BeppoSAX location and an optical transient (Hurley et al. 1997c), and numerous other BeppoSAX bursts (e.g. Hurley et al. 1998b). In each case the triangulated position was in good agreement with the known position of the source.

5. Burst Selection Criteria

We have used several selection criteria for the bursts in this catalog. The first is that the burst must have been detected by *Ulysses* and BATSE. Because of the very different detector sizes, all the bursts satisfying this criterion are observed to be rather intense by BATSE, and therefore detection by BATSE is unambiguous. However, the weaker events (as observed by *Ulysses* in the real time mode) may be difficult to identify. In these cases, we rely on several supplementary semi-empirical criteria. One is that the r_{min}^2 statistic, divided by the number of degrees of freedom, be less than unity. Another is that the maximum value of the correlation coefficient ρ be greater than 0.5. Yet another is that the ratio of *Ulysses* counts to BATSE counts lie in the range 0.019 ± 0.009 . It might seem unusual that the average value of this ratio is 0.019, whereas the ratio of the the *Ulysses* projected area in any direction to a single BATSE LAD area is closer to 0.01, and the BATSE counts are derived from at least two LAD's in this procedure. Several factors account for this. First, the *Ulysses* energy range is wider than BATSE's: 25 - 150 keV *vs.* 25 - 100 keV. Second, the *Ulysses* lower energy threshold actually allows photons with energies as low as 15 keV to be counted, albeit with lower efficiency. Third, the two *Ulysses* hemispherical detectors are thin, so photons which do not interact in one hemisphere may interact in the other, increasing the effective area. Finally, the BATSE count rates are not corrected for dead time, which is known to affect the brighter bursts (which are in general among the bursts we observe).

This set of criteria is not an absolute one. To a good approximation, every gamma-ray burst is different from every other one. In addition, data gaps, Earth occultation, telemetry noise, unusual background behavior, and different data modes complicate some analyses. In some cases, bursts satisfying all the criteria above are rejected because they are simply too weak to allow reliable triangulation. In other cases, bursts which do not satisfy one or more criteria may be accepted.

A final criterion for inclusion in this catalog is that the burst must not have been observed by a third interplanetary spacecraft. The *Ulysses* / BATSE bursts also observed by *Mars Observer* have been published in Laros et al. (1997). The *Ulysses* /BATSE bursts also observed by *Pioneer Venus Orbiter* are in press (Laros et al. 1998).

6. A Few Statistics

Over the period covered by the 3B catalog, *Ulysses* observed 346 confirmed cosmic gamma-ray bursts (i.e., bursts that were observed by at least one other spacecraft). Of these, 274 were observed by *Ulysses* and BATSE and in some cases, other spacecraft as well. ² Since BATSE observed 1122 bursts during this period, *Ulysses* observes approximately one out of every 4 BATSE bursts. Of the 274, 64 were observed by *Ulysses* in triggered mode, and 210 in real time mode.

²A list of all cosmic bursts and the spacecraft which detected them may be found at <http://ssl.berkeley.edu/ipn3/index.html>.

Finally, 220 were observed by *Ulysses* and BATSE, but not by a third interplanetary spacecraft; two of these could not be triangulated according to the criteria explained above.

The histogram of Figure 6 shows the distribution of annulus half-widths for the 218 bursts localized. The smallest is about 7 ″, the largest 32 ′, and the average is 4.5 ′. 158 of the annuli, or 72%, intersect the BATSE 1 σ error circles, whose radii are defined by $r_{1\sigma} = \sqrt{\sigma_{stat}^2 + \sigma_{sys}^2}$, where σ_{sys} is the systematic error, 1.6°, and σ_{stat} is the statistical error. Figure 5 shows one example. This is less than the number which would be predicted (87%). An analysis of a preliminary version of the IPN catalog describes several more complicated BATSE error models that are consistent with the BATSE-IPN separations (Briggs et al. 1998a). A more extensive analysis, utilizing the *Ulysses* supplement to the 4B catalog, is in progress (Briggs et al. 1998b). One quantity of interest is how close the annulus passes to the center of the error circle. Let α_1, δ_1 be the right ascension and declination of the center of a BATSE error circle, and let $\alpha_2, \delta_2, \theta_2$ be the right ascension, declination, and radius of an annulus. Then the minimum distance between the error circle and the annulus is given by $d = | \theta_2 - \cos^{-1}(\sin(\delta_1) \sin(\delta_2) + \cos(\delta_1) \cos(\delta_2) \sin(\alpha_1 - \alpha_2)) |$. A histogram of the distribution of minimum distances between the annuli and the centers of the BATSE error circles is given in Figure 7.

In general, the annuli obtained by triangulations are small circles on the celestial sphere, so their curvature, even across a relatively small BATSE error circle, is not always negligible, and a simple, four-sided error box cannot be defined. This curvature can be seen in Figure 5. For this reason, we do not cite the intersection points of the annulus with the error circle. However, we give here the formulas for finding these points for those cases where it may be useful. Let $\alpha_1, \delta_1, \theta_1$ and $\alpha_2, \delta_2, \theta_2$ be the right ascension, declination, and radii of the two small circles. Let α, δ be the right ascension and declination of the intersection points. Then

$$\sin \delta = \frac{-b \pm \sqrt{b^2 - 4ac}}{2a}$$

where

$$a = -\cos^2 \delta_1 \cos^2 \delta_2 \sin^2(\alpha_1 - \alpha_2) + 2 \sin \delta_1 \sin \delta_2 \cos \delta_1 \cos \delta_2 \cos(\alpha_1 - \alpha_2) - \sin^2 \delta_2 \cos^2 \delta_1 - \sin^2 \delta_1 \cos^2 \delta_2,$$

$$b = -2(\cos \theta_1 \sin \delta_2 + \cos \theta_2 \sin \delta_1) \cos \delta_1 \cos \delta_2 \cos(\alpha_1 - \alpha_2) + 2 \cos \theta_2 \sin \delta_2 \cos^2 \delta_1 + 2 \cos \theta_1 \sin \delta_1 \cos^2 \delta_2,$$

and

$$c = \cos^2 \delta_1 \cos^2 \delta_2 \sin^2(\alpha_1 - \alpha_2) + 2 \cos \theta_2 \cos \theta_1 \cos \delta_1 \cos \delta_2 \cos(\alpha_1 - \alpha_2) - \cos^2 \theta_2 \cos^2 \delta_1 - \cos^2 \theta_1 \cos^2 \delta_2,$$

For each of the two values of the declination δ the corresponding right ascension α is given by

$$\alpha = \alpha_1 + \cos^{-1} \frac{\cos \theta_1 - \sin \delta \sin \delta_1}{\cos \delta \cos \delta_1}$$

Figure 8 shows the BATSE peak fluxes and fluences for 162 of the 218 bursts with flux and

fluence entries in the 3B catalog. There is a slight tendency for some of the smaller fluence events to have relatively large peak fluxes over a time interval comparable to that of the *Ulysses* real time data, which helps to explain why these bursts were detected by *Ulysses*. To estimate the completeness of this catalog, we have calculated the ratios of the number of bursts detected by *Ulysses* to the number detected by BATSE above several flux and fluence thresholds starting with the weakest events in the BATSE catalog; we have used the 25-100 keV fluences in erg cm^{-2} and the peak 25 - 300 keV fluxes over 256 ms in $\text{photons cm}^{-2} \text{s}^{-1}$. Since events detected by a third spacecraft are not included in the present catalog, the numbers given represent lower limits to the completeness. Table 1 summarizes the results.

Table 1. Completeness above various thresholds

BATSE Threshold	Approximate completeness (lower limit)
$1.8 \times 10^{-9} \text{ erg cm}^{-2}$.25
$10^{-6} \text{ erg cm}^{-2}$.49
$10^{-5} \text{ erg cm}^{-2}$.74
$.27 \text{ photons cm}^{-2} \text{ s}^{-1}$.25
$1 \text{ photon cm}^{-2} \text{ s}^{-1}$.34
$10 \text{ photons cm}^{-2} \text{ s}^{-1}$.65

Finally, we have analyzed these annuli for intersections which might provide evidence of repeating bursts from a single source. Although there was a large, but statistically insignificant number of two annulus intersections, we found only one case where a three-way intersection almost occurred (BATSE bursts 451, 2286, and 2619); the data are therefore consistent with no burst repetition.

7. Table of Annuli

The ten columns in table 1 give: 1) the date of the burst, in ddmmy format, 2) the Universal Time of the burst at Earth, 3) the BATSE number for the burst, 4) the BATSE right ascension of the center of the error circle (J2000), in degrees, 5) the BATSE declination of the center of the error circle (J2000), in degrees, 6) the total 1σ statistical BATSE error circle radius, in degrees, (the approximate total 1σ radius is obtained by adding 1.6° in quadrature, but see Briggs et al. 1998a,b for an improved error model), 7) the right ascension of the center of the IPN (BATSE/*Ulysses*) annulus, epoch J2000, corrected to the heliocentric frame, in degrees, 8) the declination of the center of the IPN (BATSE/*Ulysses*) annulus, epoch J2000, corrected to the heliocentric frame, in degrees, 9) the angular radius of the IPN (BATSE/*Ulysses*) annulus, corrected to the heliocentric frame, in degrees, and 10) the half width of the IPN (BATSE/*Ulysses*) annulus, in degrees; the 3σ confidence annulus is given by $R_{IPN} \pm \delta R_{IPN}$.

This list supercedes previous ones which have been circulated in the past, but not published. The changes to it include: 1) the use of final time history and spacecraft ephemeris data; earlier lists often used preliminary and predict data, with correspondingly larger timing uncertainties, 2) transformation of annuli to heliocentric coordinates; earlier lists often gave geocentric coordinates, with correspondingly larger uncertainties in the annulus widths, 3) removal of weak events according to the criteria in section 5, 4) reprocessing of data to eliminate known clock errors, and 5) careful examination of bursts whose BATSE time histories were truncated by data gaps and Earth occultation.

Figures 9 and 10 compare the BATSE error circles with the IPN annulus/error circle intersections for the bursts in this catalog. To generate this plot, it was assumed that all annuli pass through the centers of their corresponding BATSE error circles.

We stress that while the BATSE data are for the bursts listed in the 3B catalog, the locations and error circle radii are in fact the updated ones which will appear in the 4B catalog. They have been taken from the latest online catalog, and are given here for convenience only.³ Finally, we add that 150 *Ulysses* /BATSE bursts were detected over the period between the end of the 3B

³ The catalog (<http://www.batse.msfc.nasa.gov/data/grb/4bcatalog/>) should be considered to be the ultimate source of the most up-to-date BATSE data. Table 1 is available electronically from <http://ssl.berkeley.edu/ipn3/index.html>.

catalog and the end of the 4B catalog. Analysis of these events has been completed and is being published in conjunction with the 4B catalog.

Table 2. *Ulysses* /BATSE annuli

Date	UT	N_B	$\alpha_{2000,B}$	$\delta_{2000,B}$	$\sigma_{stat,B}$	$\alpha_{2000,IPN}$	$\delta_{2000,IPN}$	R_{IPN}	δR_{IPN}
250491	00:37:46	109	91.29	-22.77	1.02	115.140	23.171	51.784	0.051
290491	03:11:50	121	174.75	14.33	1.36	116.426	22.919	59.157	0.136
020591	22:37:23	142	46.22	-52.71	0.62	297.624	-22.677	87.126	0.023
030591	07:04:13	143	87.45	38.74	0.87	117.731	22.655	30.360	0.009
110591	02:11:48	179	266.48	58.30	1.66	300.193	-22.137	83.666	0.018
230591	19:03:25	222	106.99	0.36	1.28	124.202	21.228	26.847	0.051
010691	19:22:14	249	310.12	32.34	0.17	307.035	-20.537	52.942	0.008
020691	22:55:01	257	142.76	53.99	2.06	127.387	20.448	34.526	0.163
260691	07:15:13	444	133.38	7.72	1.27	134.557	18.501	10.164	0.020
300691	07:37:02	469	304.70	35.13	0.91	315.764	-18.148	52.439	0.085
210791	19:30:12	563	315.52	-14.29	1.31	322.022	-16.198	6.769	0.436
090891	06:15:00	659	195.43	19.37	1.85	147.088	14.483	50.860	0.092
090891	19:35:45	660	281.96	64.74	2.01	327.238	-14.431	85.747	0.016
050991	23:48:55	761	360.00	-81.05	0.82	334.075	-11.942	70.787	0.017
070991	01:05:23	764	136.55	-28.23	1.30	154.322	11.849	43.573	0.131
260991	18:25:57	824	346.07	21.36	2.70	338.688	-10.171	32.155	0.294
270991	23:26:53	829	50.16	-39.65	0.34	338.937	-10.074	68.870	0.036
300991	11:55:30	841	131.80	-20.62	1.27	159.447	9.874	39.201	0.013
061091	09:01:54	871	33.30	-45.44	3.38	340.603	-9.419	50.544	0.087
221091	04:13:58	914	123.91	70.34	1.03	163.395	8.312	68.583	0.017
261091	13:07:01	938	74.68	-22.27	2.40	344.080	-8.038	80.644	0.068
061191	03:42:01	1008	343.03	-35.16	0.83	345.570	-7.445	29.223	0.023
231191	08:15:33	1114	22.81	30.34	1.14	347.386	-6.730	49.421	0.015
271191	04:22:08	1122	269.14	49.73	0.38	347.680	-6.617	88.466	0.005
071291	09:50:45	1150	307.79	29.30	1.59	348.248	-6.408	53.876	0.059
091291	18:35:58	1157	259.98	-45.08	0.40	348.333	-6.380	82.576	0.003
171291	08:22:06	1190	6.96	22.67	1.02	348.480	-6.340	35.915	0.032
211291	22:03:26	1200	215.82	-42.72	1.98	168.475	6.356	61.764	0.111
241291	11:02:58	1212	45.43	-10.79	4.68	348.444	-6.377	57.290	0.117
271291	01:05:53	1235	350.44	-68.25	0.67	348.389	-6.408	61.852	0.064
100192	09:17:58	1288	58.08	-20.80	0.42	347.700	-6.748	69.190	0.018
210292	06:14:32	1425	184.14	48.48	0.65	161.368	8.446	42.142	0.008
240292	02:43:39	1432	169.65	-66.78	2.73	160.726	8.515	75.175	0.539
270292	06:00:51	1443	68.36	66.84	1.33	160.016	8.591	83.353	0.005
070392	00:18:04	1467	355.57	-45.15	1.16	338.049	-8.795	39.316	0.066
150392	04:19:27	1484	320.58	-20.89	0.46	336.280	-8.960	16.873	0.013

Table 2—Continued

Date	UT	N_B	$\alpha_{2000,B}$	$\delta_{2000,B}$	$\sigma_{stat,B}$	$\alpha_{2000,IPN}$	$\delta_{2000,IPN}$	R_{IPN}	δR_{IPN}
070492	12:03:40	1543	341.44	-10.68	2.04	332.036	-9.187	9.927	0.437
080492	12:05:56	1545	138.96	40.83	0.58	151.890	9.190	34.380	0.022
290492	18:59:32	1571	179.08	-14.33	2.85	149.602	8.963	39.318	0.091
020592	06:02:59	1577	33.05	-17.73	1.04	329.440	-8.908	60.781	0.026
130592	16:52:39	1606	211.16	-44.77	0.65	148.956	8.591	74.250	0.005
300592	22:59:55	1630	162.68	18.13	1.67	148.993	7.901	17.618	0.070
170692	05:26:51	1652	37.66	77.51	0.51	149.807	6.977	89.064	0.012
220692	07:05:05	1663	162.10	47.17	0.31	150.169	6.667	41.336	0.005
220692	12:54:21	1664	346.81	10.01	0.55	330.187	-6.649	18.892	0.018
270692	13:02:36	1676	166.02	-2.58	0.65	150.593	6.327	23.504	0.017
010792	19:38:19	1683	314.64	33.44	0.63	330.973	-6.033	42.560	0.017
140792	20:23:26	1700	140.36	-44.64	3.28	152.298	5.079	50.262	0.099
180792	14:40:36	1708	22.44	-3.98	1.14	332.718	-4.782	49.196	0.032
180792	21:32:43	1709	296.39	-55.98	0.48	332.751	-4.760	58.948	0.004
210792	18:17:48	1717	37.55	33.49	0.73	333.083	-4.530	72.485	0.033
230792	01:00:34	1721	85.79	7.78	0.48	153.234	4.427	68.971	0.008
010892	01:16:40	1733	157.86	68.90	1.12	154.338	3.667	64.462	0.021
130892	03:33:48	1807	206.22	-28.34	1.75	155.907	2.581	63.921	0.051
140892	06:09:53	1815	258.68	-44.63	0.79	336.053	-2.478	78.143	0.006
240892	10:53:03	1872	228.59	-51.79	0.33	157.427	1.505	76.788	0.003
300892	01:45:18	1883	258.53	-73.99	0.54	338.192	-0.949	86.267	0.010
020992	00:29:05	1886	279.15	-20.70	2.29	338.594	-0.651	61.607	0.015
030992	00:49:17	1888	61.97	-68.37	0.75	338.732	-0.549	88.165	0.010
250992	21:45:16	1956	160.26	67.38	1.34	161.773	-1.864	68.233	0.020
031092	06:35:40	1974	150.32	-14.71	0.55	162.694	-2.674	19.765	0.021
091092	06:41:11	1983	120.41	-29.10	0.39	163.411	-3.345	46.240	0.003
151092	01:36:32	1989	123.04	41.69	0.95	164.066	-3.998	57.677	0.040
221092	15:20:59	1997	253.78	-12.42	0.41	164.862	-4.861	88.377	0.002
291092	12:37:56	2018	34.14	-1.57	1.67	345.514	5.651	50.169	0.045
301092	01:16:31	2020	86.16	6.86	1.75	165.561	-5.710	79.293	0.042
181192	22:11:44	2061	350.45	50.32	1.07	346.930	7.990	41.232	0.128
231192	06:18:31	2067	334.24	-53.25	0.72	347.111	8.481	64.897	0.008
031292	21:44:22	2074	233.62	21.03	0.74	167.337	-9.664	68.339	0.119
061292	18:24:19	2080	176.48	45.72	0.77	167.341	-9.975	51.667	0.029
071292	16:00:48	2083	306.33	-42.93	0.44	347.336	10.074	62.709	0.003
091292	02:40:56	2089	172.98	61.45	0.51	167.325	-10.228	68.392	0.048

Table 2—Continued

Date	UT	N_B	$\alpha_{2000,B}$	$\delta_{2000,B}$	$\sigma_{stat,B}$	$\alpha_{2000,IPN}$	$\delta_{2000,IPN}$	R_{IPN}	δR_{IPN}
091292	11:35:38	2090	332.97	-52.02	0.68	347.320	10.269	63.995	0.009
181292	02:30:02	2102	355.62	-55.31	1.76	347.091	11.168	66.903	0.076
271292	12:44:08	2106	206.33	-25.65	1.04	166.535	-12.089	39.698	0.113
301292	08:57:51	2110	19.52	17.21	0.33	346.301	12.353	32.939	0.112
301292	14:05:46	2111	150.54	28.63	1.71	166.282	-12.370	45.110	0.086
060193	15:37:39	2121	6.08	2.00	0.53	345.556	12.984	21.048	0.021
060193	19:57:15	2122	124.79	-32.62	0.68	165.536	-12.996	42.302	0.149
080193	02:28:55	2123	94.62	-30.44	0.99	165.383	-13.100	65.116	0.069
120193	03:47:31	2127	226.32	27.74	1.22	164.853	-13.415	72.911	0.021
120193	15:18:02	2128	210.10	51.92	1.02	164.786	-13.451	76.849	0.066
160193	02:47:02	2136	246.99	15.91	1.02	164.275	-13.700	88.748	0.026
270193	16:14:25	2149	310.95	-39.63	1.16	342.242	14.382	60.557	0.155
310193	18:57:12	2151	182.04	-8.24	2.16	161.406	-14.563	22.249	0.009
010293	16:41:55	2156	333.53	41.15	1.26	341.214	14.601	27.869	0.023
050293	10:10:31	2166	278.00	-45.74	5.98	340.403	14.729	83.936	0.277
170293	14:44:38	2197	117.78	0.98	2.27	157.517	-14.945	41.809	0.234
020393	21:33:17	2213	90.33	5.43	0.62	154.166	-14.821	66.384	0.016
090393	03:07:50	2228	325.41	51.73	0.72	332.605	14.648	36.594	0.012
100393	07:19:20	2232	284.35	-52.39	0.89	332.316	14.607	79.362	0.007
180393	12:29:53	2255	150.48	-18.85	1.09	150.361	-14.267	5.323	0.320
290393	03:09:25	2273	179.25	-8.65	0.94	148.090	-13.723	35.582	0.010
310393	03:11:16	2276	43.00	47.27	2.03	327.701	13.613	77.070	0.078
050493	08:54:49	2286	198.18	-8.80	0.55	146.754	-13.315	52.136	0.005
060493	07:16:25	2289	299.81	29.01	0.51	326.595	13.263	31.383	0.011
090493	04:50:10	2295	295.83	43.18	2.04	326.125	13.098	37.466	0.366
090493	21:25:40	2297	176.91	-39.75	1.25	146.019	-13.056	39.155	0.088
140493	02:27:15	2303	311.42	9.92	0.91	325.406	12.819	14.314	0.061
180493	14:38:18	2307	311.65	21.37	1.27	324.831	12.570	14.596	0.415
240493	19:19:00	2315	54.22	41.60	1.67	324.179	12.245	86.680	0.134
250493	10:17:29	2316	18.00	-35.19	0.31	324.122	12.214	70.285	0.034
260493	12:40:32	2319	67.82	10.13	1.10	144.025	-12.159	75.515	0.028
280493	01:07:12	2320	129.85	-55.45	1.68	143.900	-12.085	46.202	0.005
300493	15:01:18	2321	106.33	20.97	0.36	143.709	-11.967	50.803	0.009
020593	13:52:52	2323	254.72	-46.53	0.78	323.580	11.882	87.103	0.039
060593	14:52:51	2329	64.45	-5.97	0.24	143.364	-11.717	77.827	0.004
180593	03:20:25	2346	349.17	-37.51	1.04	323.086	11.354	53.387	0.019

Table 2—Continued

Date	UT	N_B	$\alpha_{2000,B}$	$\delta_{2000,B}$	$\sigma_{stat,B}$	$\alpha_{2000,IPN}$	$\delta_{2000,IPN}$	R_{IPN}	δR_{IPN}
230593	19:40:53	2350	14.80	4.21	2.64	323.121	11.238	44.153	0.124
310593	15:53:38	2362	340.04	13.25	2.16	323.341	11.152	15.895	0.044
090693	10:07:24	2383	208.73	-16.38	1.62	143.799	-11.158	64.377	0.132
140693	03:40:30	2393	168.14	23.95	1.15	144.132	-11.210	42.800	0.008
050793	12:39:08	2429	283.08	-39.24	0.99	326.244	11.861	65.410	0.124
060793	08:09:10	2432	210.09	-1.36	1.31	146.342	-11.898	63.498	0.045
080793	05:12:38	2433	86.55	-69.02	6.25	146.572	-11.989	62.867	0.076
090793	06:14:22	2436	194.41	-46.73	0.67	146.700	-12.042	54.525	0.028
140793	16:12:53	2446	257.70	23.70	0.97	327.399	12.344	68.720	0.048
210793	01:17:22	2452	78.66	-33.15	1.52	148.275	-12.751	66.262	0.085
210793	12:45:35	2453	298.58	-40.79	1.79	328.342	12.785	61.079	0.101
270793	08:08:29	2466	159.99	-23.89	1.28	149.185	-13.209	16.546	0.136
310793	03:16:31	2475	116.53	45.49	2.15	149.754	-13.514	66.345	0.036
050893	12:39:28	2482	334.55	-15.60	0.83	330.584	13.983	30.305	0.208
090893	05:11:04	2486	37.97	-74.63	1.79	151.166	-14.323	80.857	0.088
220893	14:44:51	2500	213.09	-0.68	2.28	153.348	-15.724	65.872	0.232
310893	09:16:05	2507	223.29	-3.63	0.47	154.815	-16.774	67.536	0.007
030993	00:19:29	2511	88.67	-10.42	4.20	155.258	-17.109	64.672	0.109
050993	03:26:30	2514	310.95	-1.22	0.63	335.615	17.389	28.629	0.006
100993	12:12:08	2522	167.59	-66.69	0.54	156.521	-18.114	48.810	0.044
140993	02:49:11	2530	34.26	34.29	1.53	337.128	18.628	50.198	0.173
160993	20:19:23	2533	280.71	65.39	0.22	337.586	19.026	57.392	0.013
220993	06:24:46	2537	271.20	55.89	0.45	338.488	19.847	67.999	0.003
270993	04:18:07	2542	108.61	-9.52	1.62	159.296	-20.624	52.084	0.115
061093	21:31:50	2566	66.31	65.28	1.70	340.850	22.262	70.461	0.049
081093	07:18:14	2570	42.98	21.37	0.85	341.069	22.510	58.202	0.082
081093	11:09:10	2571	165.40	33.93	0.86	161.094	-22.537	60.104	0.027
141093	17:01:01	2586	272.50	9.34	0.50	342.042	23.672	67.956	0.010
171093	01:17:49	2590	181.44	-83.11	0.65	162.389	-24.110	58.979	0.003
191093	18:22:34	2593	242.92	-18.70	1.66	162.779	-24.628	73.476	0.025
241093	13:29:09	2603	137.63	-8.49	0.53	163.447	-25.567	30.574	0.083
261093	11:35:57	2606	51.36	-10.56	0.48	343.704	25.955	75.482	0.087
301093	08:08:42	2609	326.41	58.24	0.55	344.202	26.745	31.863	0.058
311093	04:06:35	2611	325.10	62.73	0.32	344.306	26.918	37.073	0.005
031193	16:25:42	2617	87.88	65.05	0.31	344.732	27.657	72.278	0.008
061193	20:32:04	2619	196.75	-3.13	1.11	165.094	-28.337	40.406	0.232

Table 2—Continued

Date	UT	N_B	$\alpha_{2000,B}$	$\delta_{2000,B}$	$\sigma_{stat,B}$	$\alpha_{2000,IPN}$	$\delta_{2000,IPN}$	R_{IPN}	δR_{IPN}
121193	18:45:53	2628	311.51	55.95	0.53	345.711	29.654	34.291	0.010
261193	04:46:46	2660	157.28	70.08	3.02	346.750	32.795	80.134	0.109
261193	19:31:39	2661	3.29	-17.40	0.22	346.785	32.945	50.498	0.004
041293	09:48:10	2676	250.15	38.23	0.18	347.083	34.824	76.909	0.004
051293	14:59:51	2679	15.56	66.49	2.22	347.108	35.133	38.364	0.018
081293	04:37:19	2682	198.73	-29.93	0.56	167.142	-35.783	34.384	0.050
081293	09:34:40	2683	234.11	-40.29	3.06	167.143	-35.836	51.960	0.143
211293	02:09:50	2700	91.02	-43.17	0.50	166.799	-39.143	56.073	0.036
221293	21:21:33	2703	192.52	28.65	0.66	166.675	-39.621	73.261	0.251
251293	23:20:12	2709	4.85	9.87	0.79	346.415	40.440	35.141	0.212
261293	20:11:09	2711	205.95	21.63	2.82	166.329	-40.669	74.178	0.127
010194	22:42:00	2729	189.27	62.84	3.47	345.578	42.289	78.226	0.064
020194	02:45:52	2732	10.90	45.11	1.27	345.554	42.335	18.951	0.195
030194	22:12:56	2736	267.90	7.14	0.65	345.274	42.810	76.721	0.016
130194	16:47:54	2756	209.39	-23.16	9.65	163.289	-45.332	42.651	0.049
190194	15:44:40	2773	131.41	39.29	1.39	161.654	-46.793	89.606	0.051
280194	16:50:58	2790	224.02	-15.22	0.96	158.510	-48.816	64.647	0.059
290194	10:43:17	2793	127.46	28.59	0.82	158.217	-48.971	81.612	0.072
010294	07:40:40	2794	268.61	22.37	1.67	337.027	49.542	59.277	0.125
030294	15:46:56	2797	184.16	-40.95	0.58	156.002	-49.973	20.512	0.052
060294	00:08:37	2798	144.20	-59.96	0.15	154.922	-50.380	13.687	0.039
100294	19:13:16	2812	152.29	82.13	0.66	332.566	51.121	48.298	0.007
170294	23:02:42	2831	29.07	4.55	0.69	328.739	51.947	69.334	0.005
180294	19:32:28	2833	349.71	-19.69	0.35	328.264	52.023	73.939	0.010
280294	11:29:00	2852	127.98	-12.36	0.44	142.713	-52.495	42.173	0.012
010394	20:10:37	2855	103.51	64.35	0.35	321.919	52.509	59.400	0.029
020394	05:08:31	2856	12.49	-23.97	0.21	321.700	52.508	88.572	0.005
120394	11:28:22	2877	221.50	-56.17	0.61	135.895	-52.124	48.964	0.052
190394	23:57:20	2889	68.74	-12.60	0.39	132.014	-51.403	62.552	0.090
210394	22:05:07	2890	160.33	3.10	0.85	131.093	-51.168	58.918	0.233
230394	22:04:38	2891	213.89	8.37	0.85	310.173	50.907	85.032	0.016
280394	12:05:34	2894	97.18	-32.35	0.58	128.216	-50.236	26.692	0.028
290394	05:49:26	2895	237.51	-68.89	0.50	127.917	-50.121	51.112	0.006
290394	18:15:37	2897	204.91	-10.33	1.00	127.712	-50.040	69.434	0.026
300394	20:44:39	2899	193.80	-33.63	1.72	127.286	-49.861	48.714	0.320
060494	01:10:54	2913	225.44	-39.10	1.24	125.133	-48.806	69.435	0.043

Table 2—Continued

Date	UT	N_B	$\alpha_{2000,B}$	$\delta_{2000,B}$	$\sigma_{stat,B}$	$\alpha_{2000,IPN}$	$\delta_{2000,IPN}$	R_{IPN}	δR_{IPN}
100494	15:45:02	2919	254.89	30.80	0.93	303.788	47.974	42.261	0.047
120494	01:40:31	2922	217.17	-38.35	1.12	123.422	-47.710	58.846	0.303
140494	16:46:25	2929	181.26	-26.15	0.50	122.794	-47.222	49.154	0.026
190494	19:10:58	2940	359.86	-47.95	0.58	121.768	-46.270	73.314	0.062
290494	00:43:53	2953	35.10	-57.52	0.32	120.524	-44.594	51.727	0.006
030594	05:07:44	2958	161.00	10.06	0.60	120.195	-43.873	64.039	0.057
120594	17:37:50	2974	232.97	55.88	2.65	299.935	42.376	44.482	0.007
200594	00:21:38	2984	323.50	6.93	0.88	300.146	41.389	40.428	0.019
260594	10:55:26	2993	80.41	-30.39	0.96	120.590	-40.650	33.571	0.347
260594	20:20:05	2994	131.85	34.20	1.69	120.622	-40.611	76.690	0.012
290594	03:17:02	2998	163.64	-25.33	3.45	120.834	-40.382	35.002	0.334
290594	16:20:36	3002	66.19	-23.75	3.30	120.889	-40.330	47.443	0.021
290594	21:18:56	3003	214.84	58.93	0.46	300.908	40.314	56.125	0.083
090694	16:29:06	3024	284.14	23.34	1.01	302.269	39.513	18.866	0.118
190694	21:31:20	3035	299.05	-29.89	0.34	303.996	39.141	69.575	0.026
220694	13:18:16	3039	299.58	-31.24	0.82	304.505	39.108	72.495	0.012
230694	18:46:23	3042	108.37	75.78	0.46	304.747	39.101	65.666	0.013
010794	21:46:38	3055	145.18	-6.43	0.81	126.479	-39.199	37.139	0.157
020794	09:28:11	3056	29.73	-23.53	0.57	126.586	-39.214	78.876	0.116
030794	04:40:46	3057	131.50	27.39	1.25	126.771	-39.239	67.508	0.005
040794	23:32:07	3060	212.49	47.25	0.64	307.181	39.305	67.688	0.082
060794	19:24:33	3062	265.11	26.40	1.86	307.614	39.384	36.694	0.287
080794	20:42:06	3067	301.58	24.66	1.02	308.112	39.490	17.427	0.022
140794	12:54:21	3075	333.58	-42.10	1.59	309.555	39.862	85.495	0.067
170794	03:24:29	3087	109.80	12.93	0.71	130.246	-40.076	54.328	0.006
280794	02:55:32	3099	42.57	-49.08	0.76	133.354	-41.280	60.269	0.045
280794	14:06:40	3100	291.22	4.45	1.29	313.491	41.344	44.189	0.181
280794	23:58:54	3101	85.49	-39.87	1.44	133.620	-41.397	36.263	0.066
060894	04:38:48	3108	276.21	-31.33	10.69	316.177	42.651	86.962	0.079
060894	09:32:56	3109	242.38	13.65	1.22	316.242	42.686	69.105	0.126
100894	02:22:42	3115	212.01	-17.47	0.53	137.468	-43.347	67.696	0.009
120894	00:27:42	3119	340.49	-46.12	2.23	138.120	-43.715	86.692	0.263
170894	08:40:15	3128	280.84	3.47	0.40	319.994	44.823	53.907	0.010
210894	21:51:27	3131	294.69	43.48	1.77	321.670	45.864	16.142	0.191
260894	20:55:20	3138	93.59	-34.63	0.45	143.593	-47.103	37.845	0.013
300894	08:59:56	3143	193.66	25.66	1.58	145.011	-48.048	89.313	0.042

Table 2—Continued

Date	UT	N_B	$\alpha_{2000,B}$	$\delta_{2000,B}$	$\sigma_{stat,B}$	$\alpha_{2000,IPN}$	$\delta_{2000,IPN}$	R_{IPN}	δR_{IPN}
100994	19:31:24	3163	332.01	-34.11	0.94	330.099	51.525	87.032	0.065
150994	06:52:19	3168	219.42	47.70	4.53	332.318	53.052	62.836	0.393

8. Acknowledgments

Support for the *Ulysses* GRB experiment is provided by JPL Contract 958056. Joint analysis of *Ulysses* and BATSE data is supported by NASA Grant NAG 5-1560. CK acknowledges support from NASA Grant NAG5-2560.

REFERENCES

- Briggs, M., Pendleton, G., Brainerd, J., Connaughton, V., Kippen, R. M., Meegan, C., and Hurley, K. 1998a, in *Gamma-Ray Bursts: 4th Huntsville Symposium*, eds. C. Meegan, R. Preece, and T. Koshut, (AIP: New York), p. 104
- Briggs, M., et al. 1998b, *ApJS*, in press
- Galama, T., et al. 1997, *ApJ*, 486, L5
- Hurley, K. 1994, in *Gamma-Ray Bursts - Second Workshop*, eds. J. Fishman, J. Brainerd, and K. Hurley, *AIP Conference Proceedings* 307 (AIP: New York), 682
- Hurley, K., et al. 1992, *Astron. Astrophys. Suppl. Ser.*, 92(2), 401
- Hurley, K., et al. 1996, *BAAS*, 28(4), 1408
- Hurley, K., et al. 1997a, *ApJ*, 479, L113
- Hurley, K., et al. 1997b, *Proc. 25th ICRC, Durban, South Africa*, OG 2.2.6, 45
- Hurley, K., et al. 1997c, *ApJ*, 485, L1
- Hurley, K., et al. 1998a, in *Gamma-Ray Bursts: 4th Huntsville Symposium*, eds. C. Meegan, R. Preece, and T. Koshut, (AIP: New York), p. 50
- Hurley, K., et al. 1998b, in *The Active X-Ray Sky: Results from BeppoSAX and Rossi-XTE*, eds. L. Scarsi, H. Bradt, P. Giommi, and F. Fiore, *Nucl. Phys. B (Proceedings Supplement)*, 69(1-3), p.660
- Kippen, M., Hurley, K., and Pendleton, G. 1998, in *Gamma-Ray Bursts: 4th Huntsville Symposium*, eds. C. Meegan, R. Preece, and T. Koshut, (AIP: New York), p. 114
- Kolatt, T., and Piran, T. 1996, *ApJ*, 467, L41
- Kulkarni, S., et al. 1998, *Nature*, 393, 35
- Laros, J., et al., 1997, *ApJS*, 110, 157
- Laros, J., et al., 1998, *ApJS*, accepted
- Meegan, C., et al., 1996, *ApJS*, 106, 45
- Metzger, M., et al., 1997, *Nature*, 387, 878
- Paczynski, B. 1991, *Acta Astronomica*, 41, 257
- Schartel, N., Andernach, H., and Greiner, J. 1997, *A&A*, 323, 659
- Struble, M., and Rood, H. 1997, *ApJ*, 490, 109
- Tokanai, F., et al. 1997, *PASJ*, 49, 207

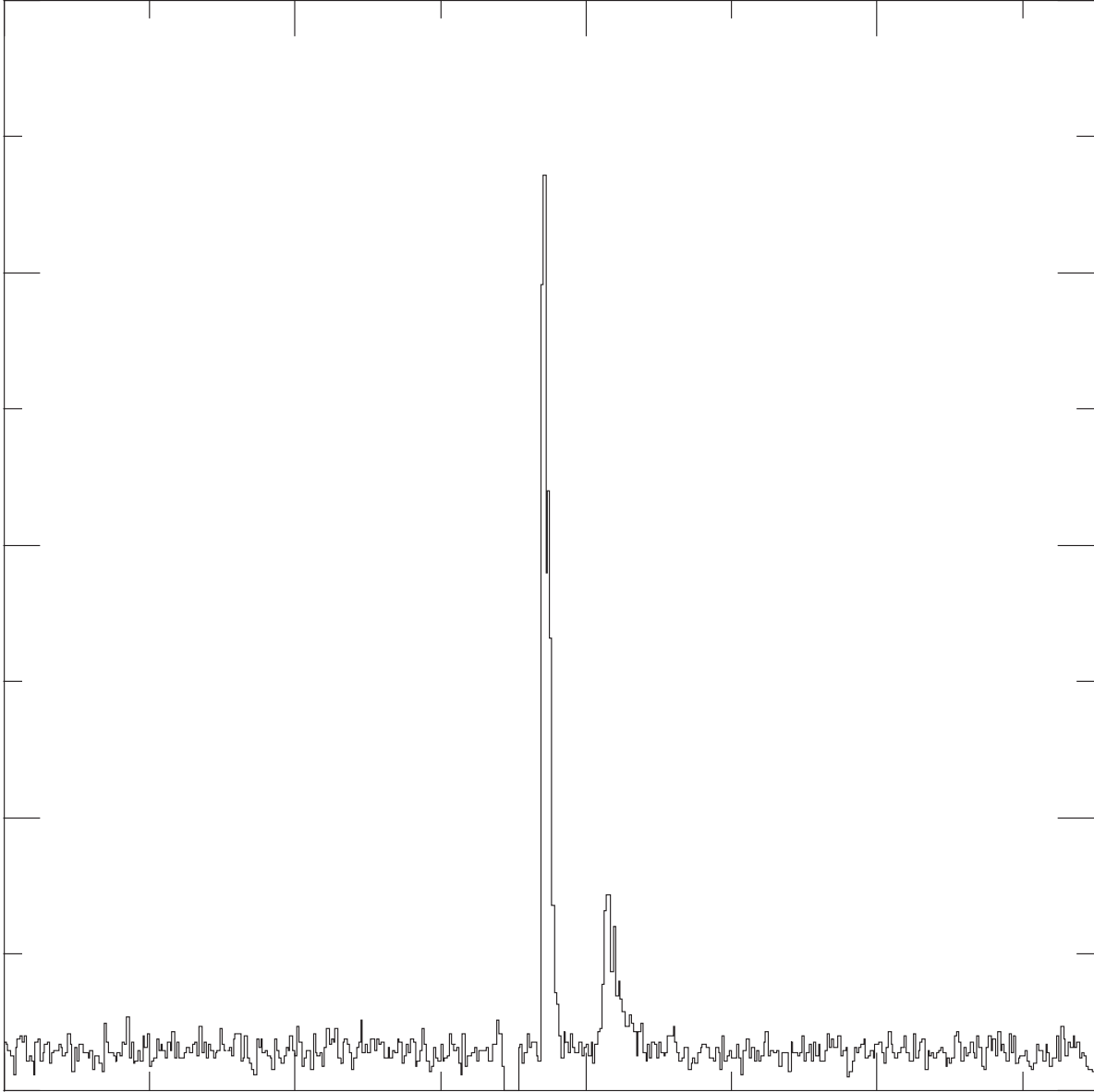


Fig. 1.— *Ulysses* triggered data. The response to BATSE burst 2151 on 1993 January 31 is shown. The time resolution is 0.03125 s.

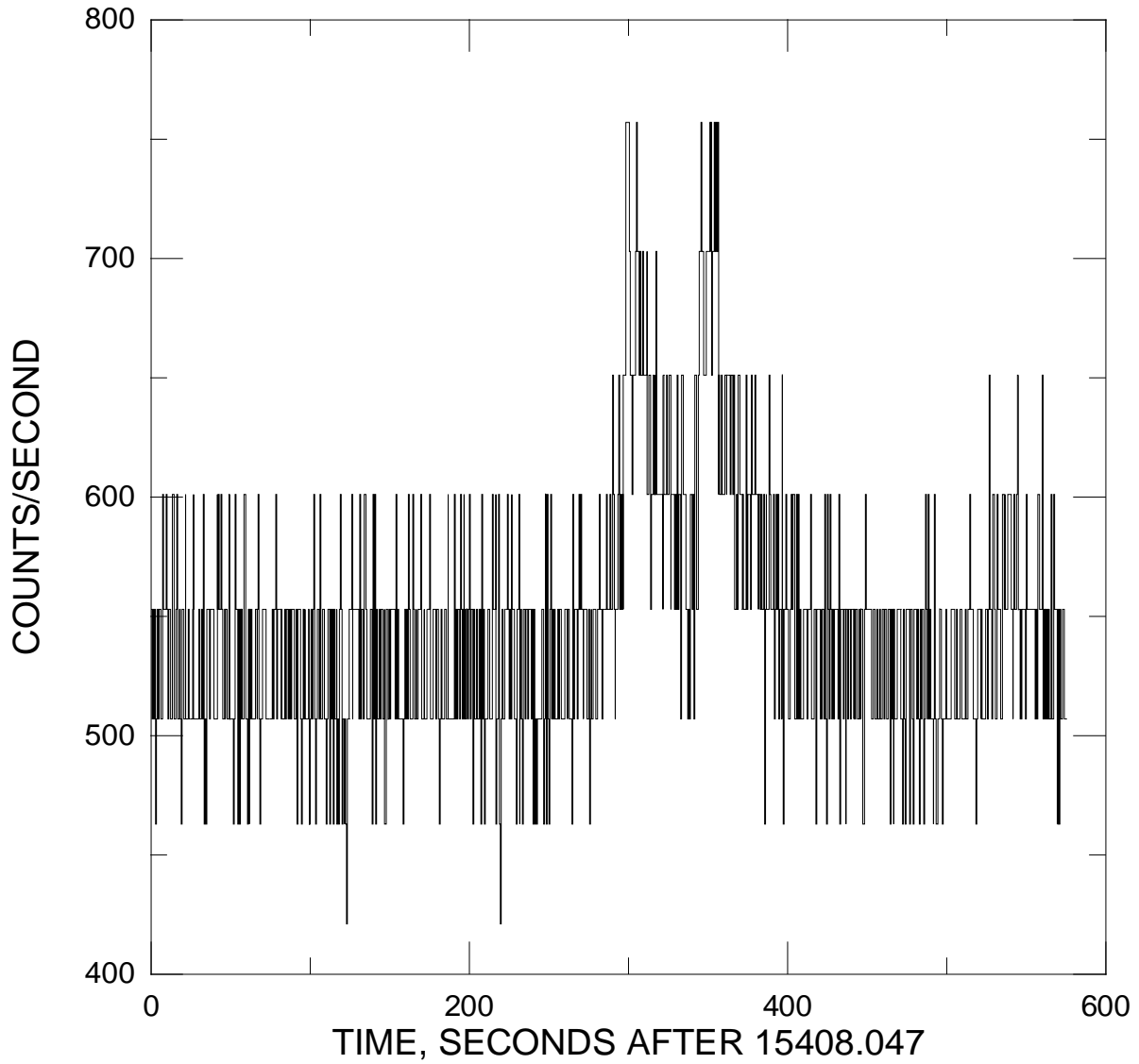


Fig. 2.— *Ulysses* GRB 0.5 s resolution real time data for the crossing window for BATSE burst 1008 on 1991 November 6. BATSE observed only the first peak of this event before entering the South Atlantic Anomaly. *Ulysses* GRB triggered on the second peak. The “quantized” appearance of the data is due to compression.

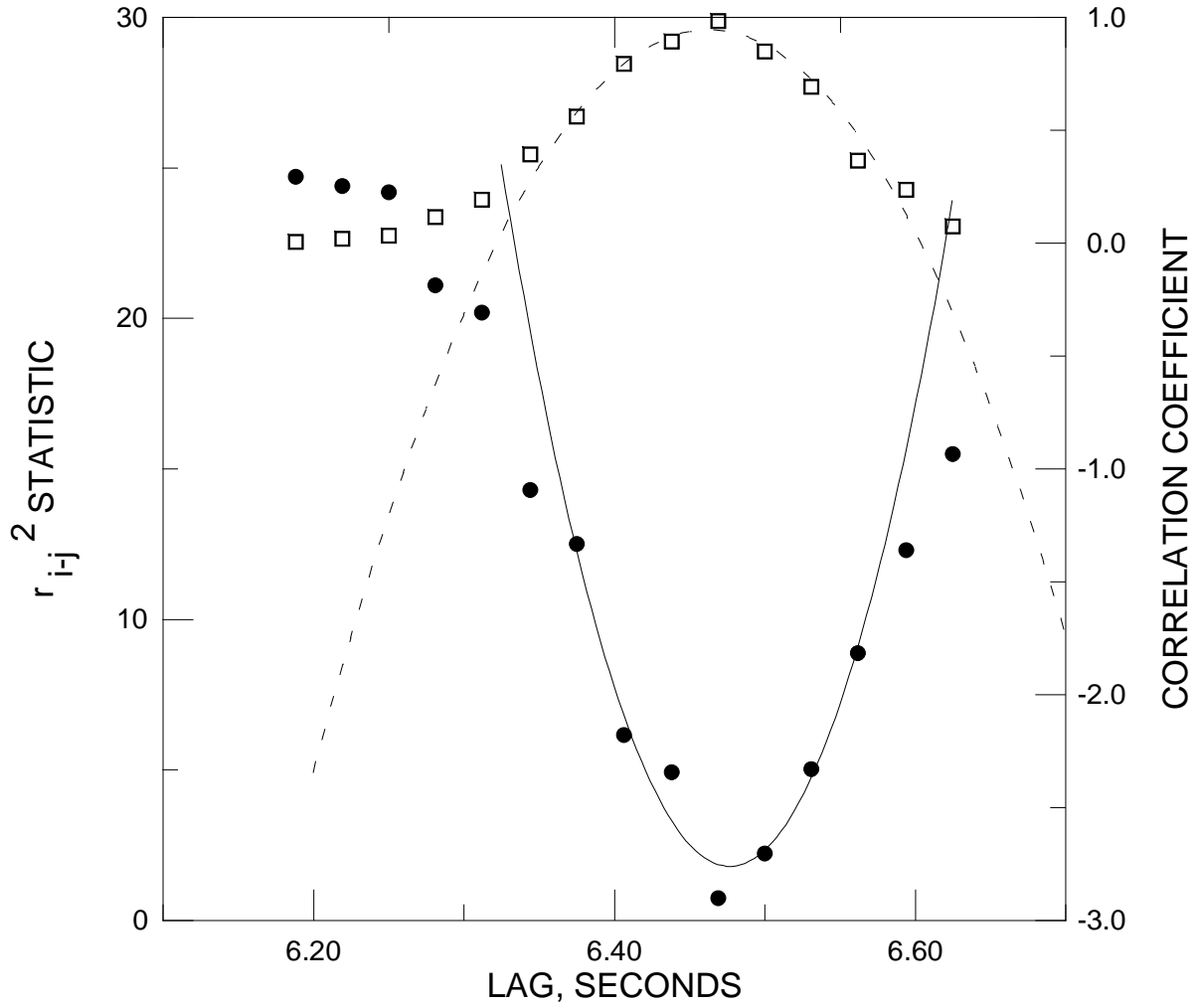


Fig. 3.— r^2_{i-j} (dots) and correlation coefficient ρ_{ij} (squares) as a function of lag for the burst of Figure 1, and their parabolic fits. The 3σ confidence interval corresponds to ≈ 6 ms.

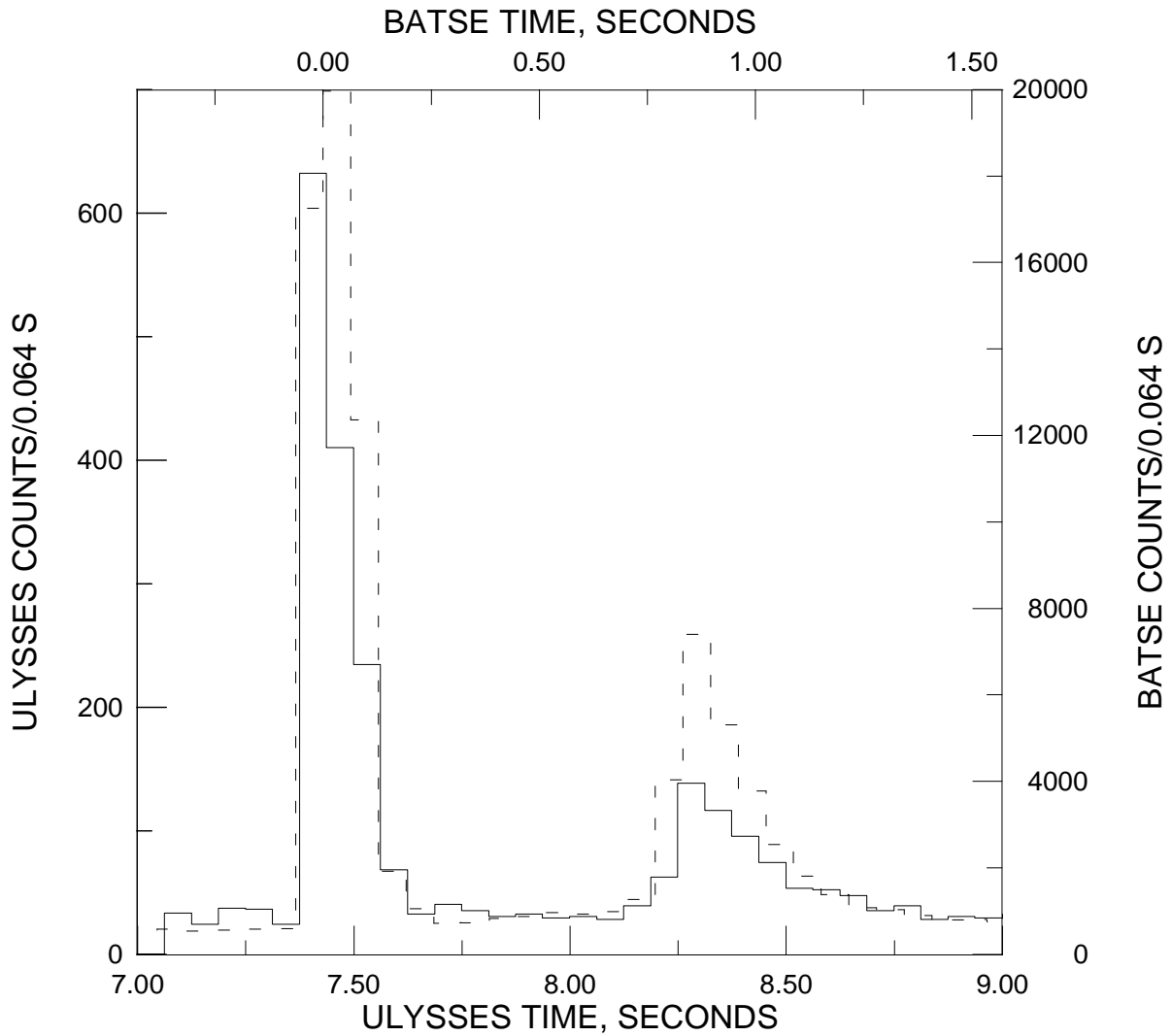


Fig. 4.— *Ulysses* (solid line) and BATSE (dashed line) time histories aligned for the best fit, for the burst of Figure 1. The BATSE data are summed over 4 LAD's and are not corrected for deadtime.

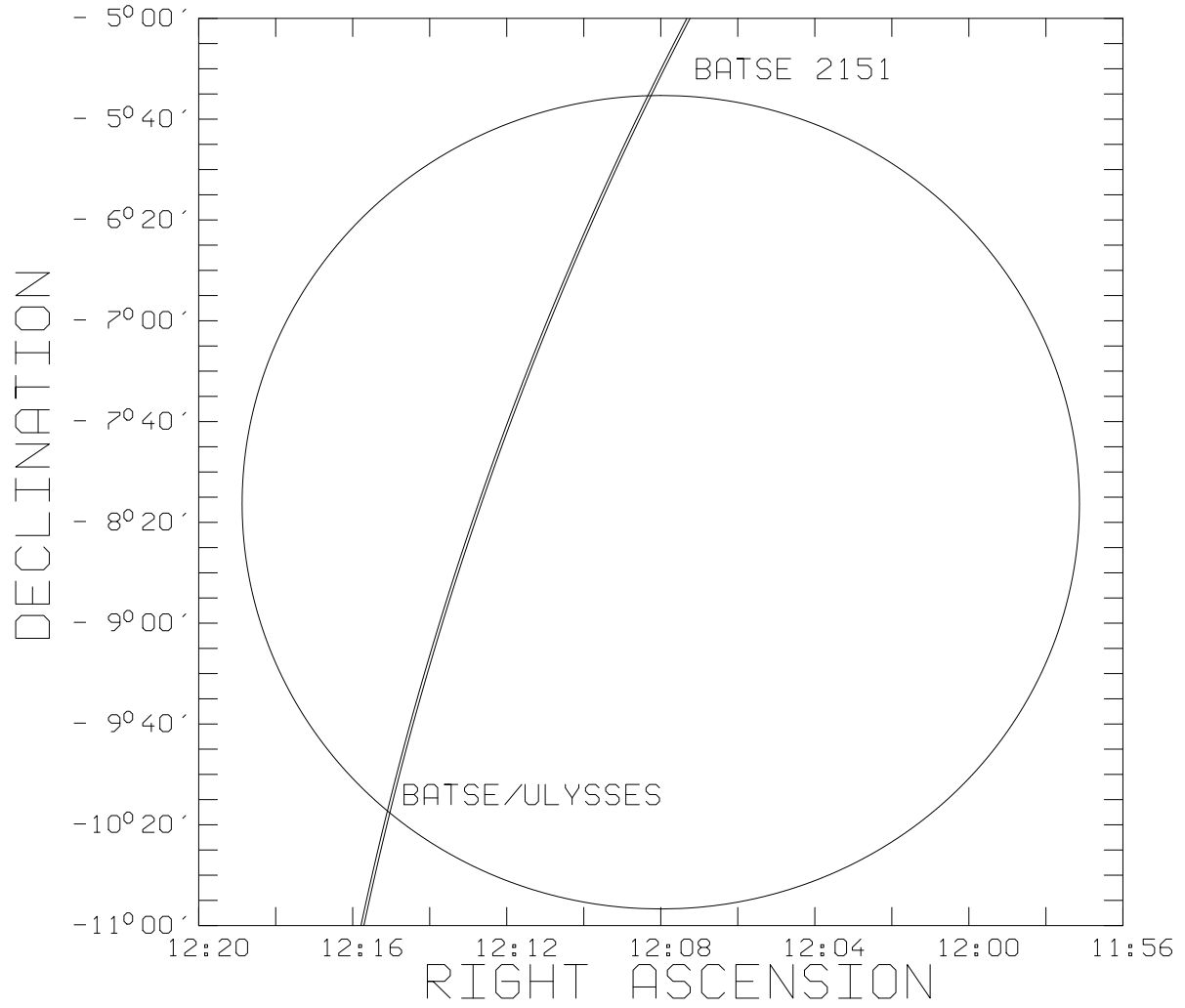


Fig. 5.— The *Ulysses* /BATSE triangulation annulus for the burst of Figure 1, and the BATSE error circle.

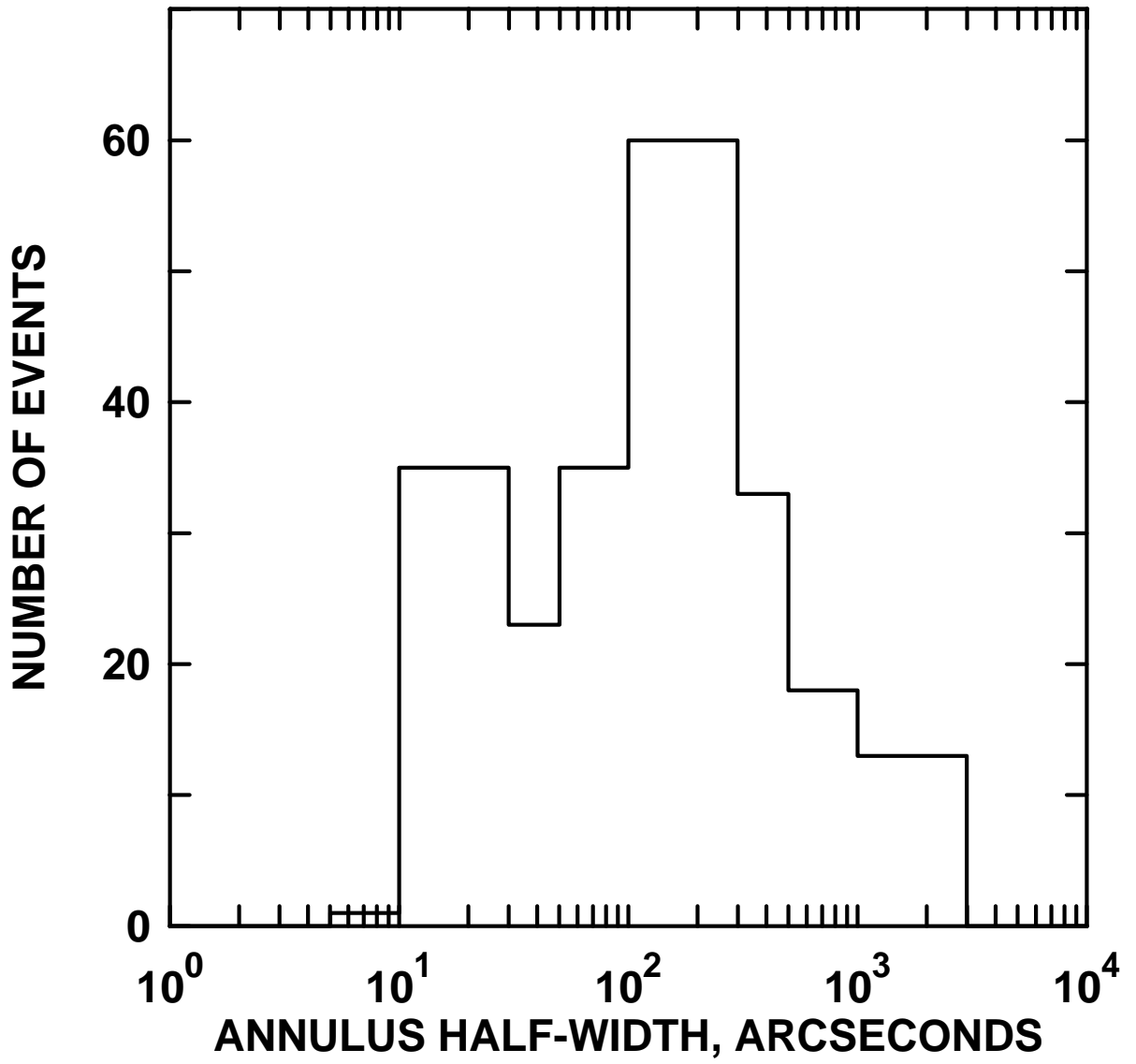


Fig. 6.— Distribution of 218 *Ulysses* /BATSE annulus half-widths (i.e., δR_{IPN} in Table 1).

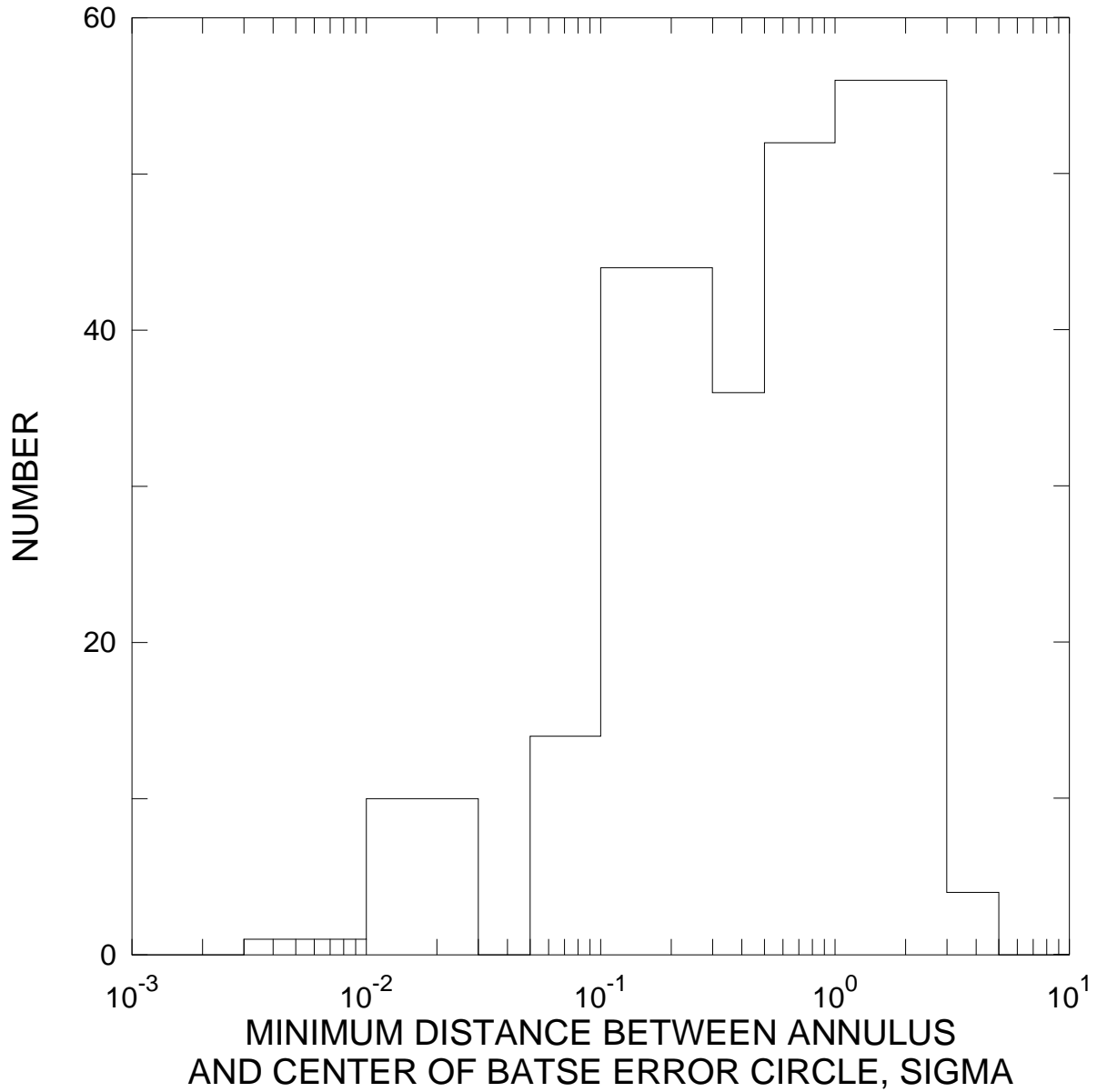


Fig. 7.— Distribution of minimum angular distances between the 218 annuli and the centers of the BATSE error circles. The angular distances are expressed in number of sigma for the BATSE error circle radii, i.e. $d/r_{1\sigma}$.

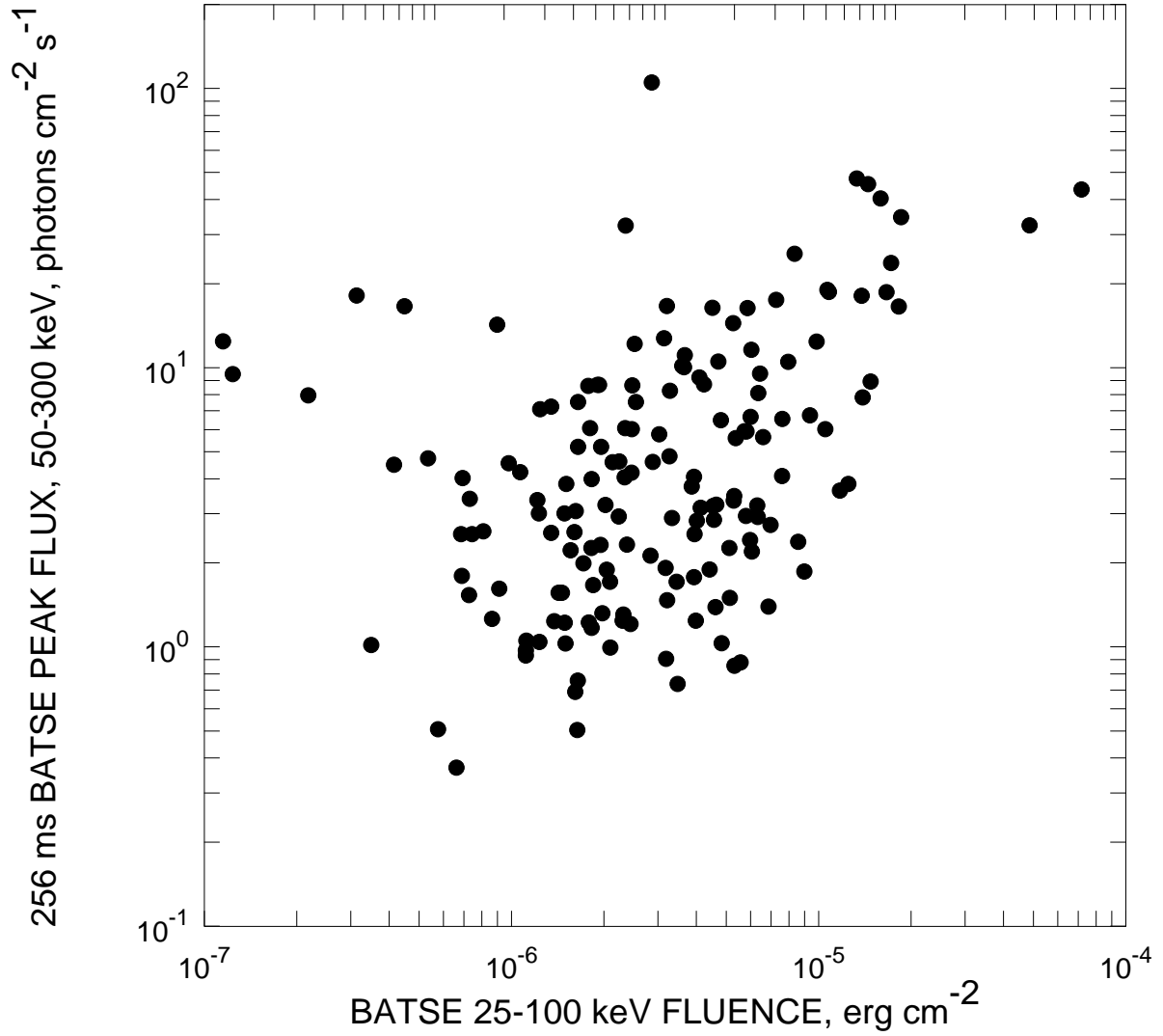


Fig. 8.— Peak fluxes (measured over 256 ms, 50-300 keV) and 25-100 keV fluences of 162 of the bursts in this catalog. No entries are given in the 3B catalog for 56 of the bursts.

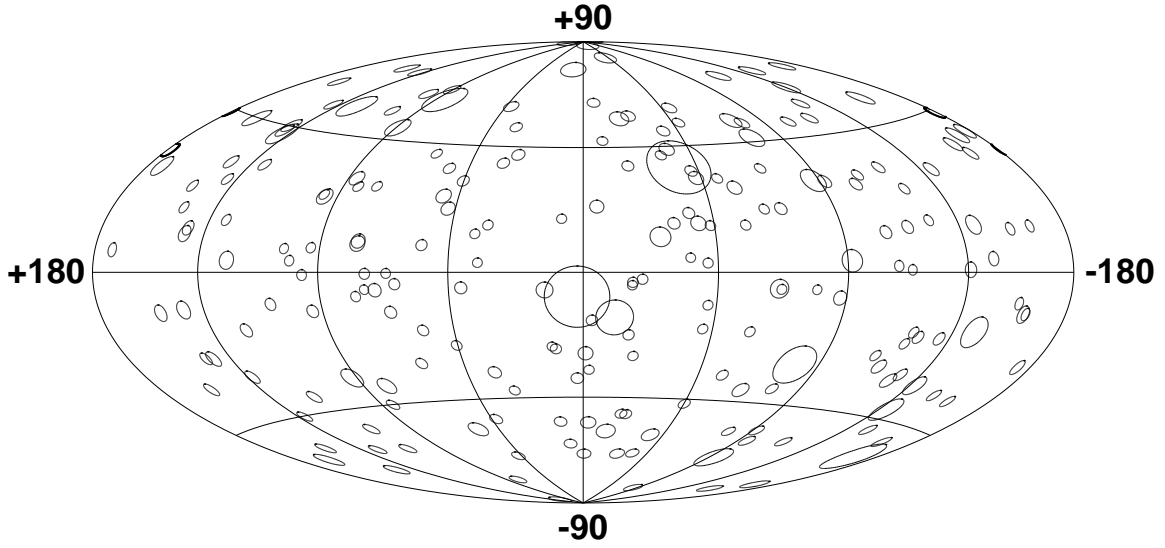


Fig. 9.— Distribution of 218 BATSE 3B error circles in galactic coordinates.

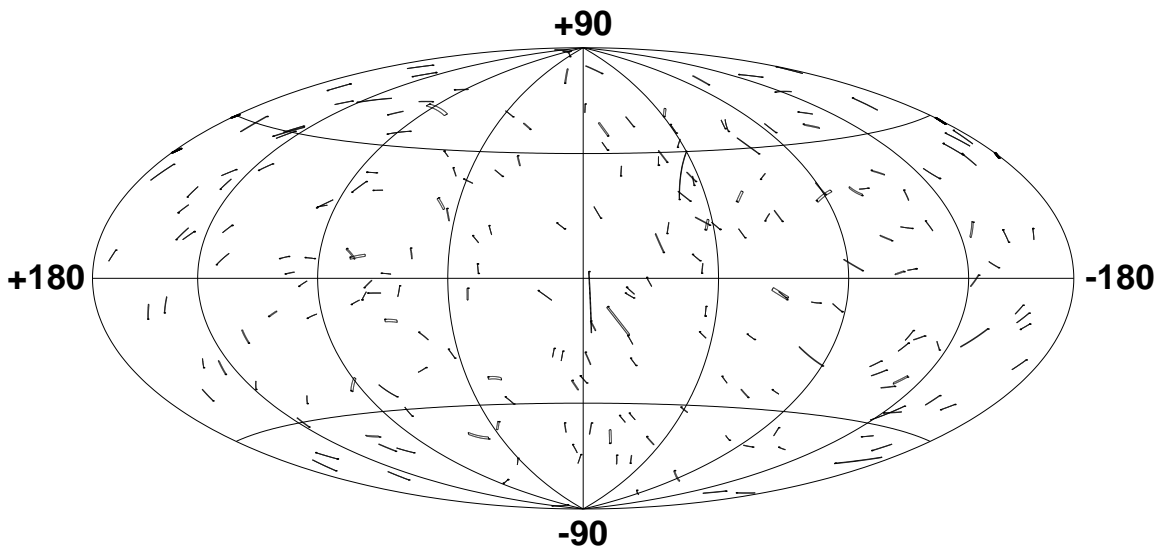


Fig. 10.— Distribution of 218 *Ulysses* /BATSE error circle/annulus intersections.